# Femtosecond spectral pulse shaping with holographic gratings recorded in photopolymerizable glasses

**M. P. Hernández-Garay,[1,*] O. Martínez-Matos,[1] J. G. Izquierdo,[2] M. L. Calvo,[1] P. Vaveliuk,[1,3] P. Cheben,[4] L. Bañares[2]**

[1] *Departamento de Óptica, Grupo Interdisciplinario de Computación Óptica (GICO-UCM,) Facultad de Ciencias Físicas, Universidad Complutense de Madrid, Avda. Complutense S/N, 28040, Madrid, Spain*

[2] *Departamento de Química Física I, Facultad de Ciencias Químicas, Universidad Complutense de Madrid, Avda. Complutense S/N, 28040, Madrid, Spain*

[3] *Faculdade de Tecnologia, Servicio Nacional de Aprendizagem Industrial SENAI-Cimatec, Avenida Orlando Gomes 1845 41650-010, Salvador, Bahia, Brazil*

[4] *Institute for Microstructural Sciences, National Research Council Canada, 1200 Montreal Road, Ottawa, Ontario K1AR6, Canada*

**mpgaray@fis.ucm.es*

**Abstract**: The majority of the applications of ultrashort laser pulses require a control of its spectral bandwidth. In this paper we show the capability of volume phase holographic gratings recorded in photopolymerizable glasses for spectral pulse reshaping of ultrashort laser pulses originated in an Amplified Ti: Sapphire laser system and its second harmonic. Gratings with high laser induce damage threshold (LIDT) allowing wide spectral bandwidth operability satisfy these demands. We have performed LIDT testing in the photopolymerizable glass showing that the sample remains unaltered after more than 10 million pulses with 0,75 TW/cm$^2$ at 1 KHz repetition rate. Furthermore, it has been developed a theoretical model, as an extension of the Kogelnik's theory, providing key gratings design for bandwidth operability. The main features of the diffracted beams are in agreement with the model, showing that non-linear effects are negligible in this material up to the fluence threshold for laser induced damage. The high versatility of the grating design along with the excellent LIDT indicates that this material is a promising candidate for ultrashort laser pulses manipulations.

©2011 Optical Society of America

**OCIS codes:** (090.0090) Holography; (090.7330) Volume gratings.

## References and links

1. M. E. Fermann, A. Galvanauskas, and G. Sucha, eds., *Ultrafast Lasers Technology and Applications*, (Marcel Dekker Inc. New York, USA, 2003).
2. C. E. Webb, and J. D. C. Jones, *Handbook of Laser Technology and Applications* (Institute of Physic publishing, USA, 2004), Chap. 2.3.5. See also: *Handbook of Optics* (McGraw-Hill Co. Third Ed., Vol. II, 2010), Chap. 20.
3. F. C. De Schryver, S. De Feyter, and G. Schweitzer, eds., *Femtochemistry*, (Wiley-VCH GmbH, Weinheim, Germany, 2001).
4. H. Ahmed, Zewail, *Physical Biology from Atoms to Medicine* (Imperial College Press, London, UK, 2008).
5. R. R. Gattass, and E. Mazur, "Femtosecond laser micromachining in transparent materials," Nat. Photonics **2**(4), 219–225 (2008).
6. M. Andrew, Weiner, *Ultrafast Optics* (John Wiley & Sons, Ltd, New Jersey, USA, 2009).
7. K. Bezuhanov, A. Dreischuh, G. G. Paulus, M. G. Schätzel, and H. Walther, "Vortices in femtosecond laser fields," Opt. Lett. **29**(16), 1942–1944 (2004).
8. O. Martínez-Matos, J. A. Rodrigo, M. P. Hernández-Garay, J. G. Izquierdo, R. Weigand, M. L. Calvo, P. Cheben, P. Vaveliuk, and L. Bañares, "Generation of femtosecond paraxial beams with arbitrary spatial distribution," Opt. Lett. **35**(5), 652–654 (2010).

#136396 - $15.00 USD Received 11 Oct 2010; revised 3 Dec 2010; accepted 6 Dec 2010; published 13 Jan 2011
(C) 2011 OSA

9. O. V. Andreeva, V. G. Bespalov, V. N. Vasil'ev, A. A. Gorodetskiĭ, A. P. Kushnarenko, G. V. Lukomskiĭ, and A. A. Paramonov, "Investigation of the spectral selectivity of volume holograms with femtosecond pulsed radiation," Opt. Spect. **96**(2), 157–162 (2004).
10. W. Wilson, A. Hoskins, M. Ayres, A. Hill, and K. Curtis, *Introduction to Holographic Data Recording, in Holographic Data Storage: From Theory to Practical Systems*, K. Curtis, L. Dhar, A. Hill, W. Wilson and M. Ayres, eds., (John Wiley & Sons, Ltd, Chichester, UK., 2010).
11. A. Villamarín, J. Atencia, M. V. Collados, and M. Quintanilla, "Characterization of transmission volume holographic gratings recorded in Slavich PFG04 dichromated gelatin plates," Appl. Opt. **48**(22), 4348–4353 (2009).
12. O. M. Efimov, L. B. Glebov, L. N. Glebova, K. C. Richardson, and V. I. Smirnov, "High-efficiency bragg gratings in photothermorefractive glass," Appl. Opt. **38**(4), 619–627 (1999).
13. R. Kashyap, *Fiber Bragg Gratings* (Elsevier, USA, 1999).
14. P. Rambo, J. Schwarz, and I. Smith, "Development of a mirror backed volume phase grating with potential for large aperture and high damage threshold," Opt. Commun. **260**(2), 403–414 (2006).
15. H. Li, H. Xiong, and Y. Tang, "Study on the laser-induced damage threshold of sol-gel $ZO_2$-PVP coating," Chin. Opt. Lett. **8**(2), 241–243 (2010).
16. B. C. Stuart, M. D. Feit, S. Herman, A. M. Rubenchik, B. W. Shore, and M. D. Perry, "Nanosecond-to-femtosecond laser-induced breakdown in dielectrics," Phys. Rev. B Condens. Matter **53**(4), 1749–1761 (1996).
17. M. D. Perry, R. D. Boyd, J. A. Britten, D. Decker, B. W. Shore, C. Shannon, and E. Shults, "High-efficiency multilayer dielectric diffraction gratings," Opt. Lett. **20**(8), 940–942 (1995).
18. B. W. Shore, M. D. Perry, J. A. Britten, R. D. Boyd, M. D. Feit, H. T. Nguyen, R. Chow, G. E. Loomis, and L. Li, "Design of high-efficiency dielectric reflection gratings," J. Opt. Soc. Am. A **14**(5), 1124–1136 (1997).
19. F. del Monte, O. Martínez-Matos, J. A. Rodrigo, M. L. Calvo, and P. Cheben, "A Volume Holographic Sol-Gel Material with Large Enhancement of Dynamic Range by Incorporation of High Refractive Index Species," Adv. Mater. **18**(15), 2014–2017 (2006).
20. P. Cheben, and M. L. Calvo, "A photopolymerizable glass with diffraction efficiency near 100% for holographic storage," Appl. Phys. Lett. **78**(11), 1490–1492 (2001).
21. O. Martínez-Matos, M. L. Calvo, J. A. Rodrigo, P. Cheben, and F. del Monte, "Diffusion study in tailored gratings recorded in photopolymer glass with high refractive index species," Appl. Phys. Lett. **91**(14), 1411151–1411153 (2007).
22. M. L. Calvo, and P. Cheben, "Photopolymerizable sol–gel nanocomposites for holographic recording," J. Opt. A, Pure Appl. Opt. **11**(2), 1–11 (2009).
23. O. Martínez-Matos, J. A. Rodrigo, M. L. Calvo, and P. Cheben, "Polarization and phase-shift properties of high spatial frequency holographic gratings in a photopolymerizable glass," Opt. Lett. **34**(4), 485–487 (2009).
24. H. Kogelnik, "Coupled Wave Theory for Thick Hologram Gratings," Bell Syst. Tech. J. **48**, 2909–2947 (1969).
25. M. G. Moharam, and L. Young, "Criterion for Bragg and Raman-Nath diffraction regimes," Appl. Opt. **17**(11), 1757–1759 (1978).
26. E. A. Bahaa Saleh and M. C. Teich, *Fundamental of Photonics*, (John Wiley & Sons eds., USA, 2007), Chap.22.
27. C. B. Schaffer, A. Brodeur, and E. Mazur, "Laser-induced breakdown and damage in bulk transparent materials induced by tightly-focused femtosecond laser pulses," Meas. Sci. Technol. **12**(11), 1784–1794 (2001).
28. A. C. Tien, S. Backus, H. Kapteyn, M. Murnane, and G. Mourou, "Short-Pulse Laser Damage in Transparent Materials as a Function of Pulse Duration," Phys. Rev. Lett. **82**(19), 3883–3886 (1999).

## 1. Introduction

The interest in ultrashort laser pulses began with the invention of the laser and has been one of continuous progress toward shorter time scales [1]. The ultrashort lasers are applied in fundamental areas of physics [2], chemistry [3], biology and medicine [4] and they are on the verge of opening up a large variety of engineering and industrial applications [1,2,5]. The unique physical properties of the high power ultrashort laser pulses rely on the broad power spectral bandwidths and in the well-defined spectral correlation. Both properties can be modified for temporal, spatial and spectral pulse shaping.

Optical elements for ultrashort pulses manipulation can be divided in two groups, according to how they process the spectrum, and therefore, which pulse application are involved. The first group is established by the optical elements for temporal [6] and spatial pulse shaping [7,8]. They must preserve the complete spectrum and operate as dispersive elements in order to adjust the spectral phase for pulse envelope control. The second group is formed by the optical elements capable to perform wavelengths selectivity in the broad spectral bandwidths of the pulses [9]. These elements are variable spectral filters, which should preserve the correlation of the spectral phase to maintain the pulse character [6].

#136396 - $15.00 USD Received 11 Oct 2010; revised 3 Dec 2010; accepted 6 Dec 2010; published 13 Jan 2011
(C) 2011 OSA

Diffraction gratings are ideal candidates to satisfy the demands of the two groups. They are dispersive optical elements that maintain the spectral phase correlation of the pulse and they can be designed to have variable bandwidth operability. The grating bandwidth can be selected to preserve or filtering the pulse spectrum according to the demanded application. Diffraction gratings recorded by holographic methods [10] exhibit special features compared to standard gratings fabricated by mechanical methods. They are defect-free periodic structures that allow high versatility design together with an easy implementation. Some representative diffractive elements implemented in photosensitive materials for ultrashort laser pulse manipulation have been reported in the literature. The dichromated gelatin holographic gratings [11] are probably the best-known type of holographic optical elements applied in ultrashort laser. Other elements such as photothermal refractive gratings [12] and fiber Bragg gratings [13] have also been proposed. Mirror backed volume phase gratings with coated sol-gel or dichromated gelatin films are applied for telecommunication and pulse compression [14–16], whereas surface relief reflection gratings [17,18] are readily available from commercial sources. However, no report exist treating photosensitive materials which simultaneously satisfy the two groups above mentioned together with a high laser-induced damage threshold. In this paper we demonstrate the capability of volume phase holographic gratings (VPHG) recorded in photopolymerizable glasses to preserve or filtering the incoming pulse spectrum exhibiting an excellent damage threshold.

The paper is organized as follows: in Section 2 we report the properties of the holographic gratings recorded in photopolymerizable glasses; in Section 3 we develop a theoretical model to explain the main features of the diffracted pulses and we find a suitable relation between grating parameters for spectral pulse shaping; in Section 4 is analyzed the diffraction efficiency, as well as the spectral properties of the diffracted laser beams when ultrashort pulses of 50 fs duration centered at 800 nm and 400 nm impinge onto the gratings; in Section 5 we explore the laser induced damage threshold (LIDT) of the photopolymerizable glasses and the work ends with concluding remarks in Section 6.

## 2. Holographic gratings

The photosensitive material used in this work [19] is a modified composition of a highly efficient photopolymerizable sol-gel glass synthesized earlier by Cheben et al. [20], wherein the modification is achieved by incorporating the Zr-based high refractive index species (HRIS) at molecular level [19,21,22]. The sol-gel technique, applied to the synthesis of the material, permits to cast samples with wide thickness design with a low scattering coefficient of 1.2 x $10^{-3}$ $\mu m^{-1}$ [19,22]. The samples were encapsulated between two coverglasses of 150 μm thickness providing an optical contact between the holographic recording material and the coverglasses.

The VPHGs formation is obtained by the interference of two mutually coherent s-polarized writing beams, using a continuous wave (cw) frequency-doubled Nd:YAG laser at 532 nm. The writing beams were incident on the sample in an unslanted configuration, intersecting the latter at different angles with respect to the sample normal, as is described in [21,23]. Thus, interference fringes in this work are formed with various spatial frequencies ranging from 500 to 4000 lines/mm. Properties of the gratings has been characterized extensively for monochromatic light demonstrating an excellent optical performance and a negligible surface modulation, as it is shown in references [19–23]. The grating thickness is measured directly on the sample and the refractive index modulation is calculated fitting the diffraction efficiency of one of the writing beams under Bragg angle to Kogelnik's coupled wave theory [24]. In this paper we extend the grating characterization to ultrashort laser pulses. The value of the Klein-Cook parameter $Q$ [25]

$$Q = \frac{2\pi\lambda_c T}{n_0 \Lambda^2}, \tag{1}$$

#136396 - $15.00 USD Received 11 Oct 2010; revised 3 Dec 2010; accepted 6 Dec 2010; published 13 Jan 2011
(C) 2011 OSA

defines the grating regimen according to the diffraction properties. For $Q > 10$ the VPHG operates as a thick hologram under the Bragg regime. $T$, $\Lambda$, $n_0$ and $\lambda_c$ are the grating thickness, the grating period, the background value of the refractive index of the grating and the central wavelength of the pulsed laser, respectively. In Section 3 we will demonstrate a suitable relation between $Q$ and the grating bandwidth operations (see (7)). Therefore, $Q$ determines the grating tolerance to out-Bragg detuning and is the key parameter to design the grating bandwidth operability. Appropriate values of $Q$ will preserve or filtering the spectrum of the incoming pulses.

### 3. Theoretical model

In this section we generalize the one dimensional Kogelnik's coupled wave theory [24] to the case of polychromatic light, by including pulses with broad spectral bandwidths. We analyze the particular case of transmission VPHGs composed by unslanted planes perpendicular to the grating interphase. We start from the following assumptions:

1) The gratings are encapsulated between two dispersive coverglasses ($n_o(\lambda)$) providing optical contact, as indicated in Section 2. The optical element (grating and coverglasses) is embedded in a non-dispersive medium with refraction index $n = 1$ (in the air).

2) The light dispersion in the optical element mainly occurs at the interface air-coverglass since the refractive index of the grating and the coverglasess are similar (~1.52). Therefore, once the light is dispersed it maintains the direction of propagation along the optical element without noticeable change. As a first approximation we consider an unique background refractive index for the coverglasess and the gratings, equal to $n_o(\lambda)$.

3) The refractive index modulation $\Delta n$ fulfills $\Delta n << n_o(\lambda)$. Hence, $\Delta n$ can be considered as a constant for the wavelength range of interest.

4) The ultrashort pulsed plane wave can be described as a superposition of monochromatic planes waves propagating in the same direction in the air. The complex amplitude of each component is obtained by the Fourier Transform of its time-dependent electric field [26].

5) The monochromatic components of the pulse impinge onto the grating under the same incidence angle $\theta_i$. Snell's refraction law applied to the interface air-coverglass $\sin\theta_i = n_o(\lambda)\sin\theta(\theta_i,\lambda)$, defines the incidence angle $\theta(\theta_i,\lambda)$ inside the grating for each spectral component according to 2).

6) Each individual monochromatic plane wave behaves independently [26] according the Kogelnik's coupled waves theory [24].

The coupled wave theory analyzes the diffraction efficiency originated by a grating when an incoming monochromatic plane wave impinges onto the sample under-Bragg angle as well as off-Bragg angle. The detuning from Bragg condition was analyzed only for two individual cases. First, monochromatic light with angle of incidence mismatch and second, collinear polychromatic light propagation inside the grating, with light wavelength mismatch. We extend this theory to a general case in which we place ourselves in the regime of point 5): the angle and wavelength mismatch occurs simultaneously. We refer to this case as the generalized mismatch condition, and it can be defined through the function $\vartheta(\theta_i,\lambda)$ [24]:

$$\vartheta(\theta_i,\lambda) = \frac{2\pi\sin\theta(\theta_i,\lambda)}{\Lambda} - \frac{\pi\lambda}{n_0(\lambda)\Lambda^2}. \qquad (2)$$

#136396 - $15.00 USD Received 11 Oct 2010; revised 3 Dec 2010; accepted 6 Dec 2010; published 13 Jan 2011
(C) 2011 OSA

This equation depends on the grating parameters, on the incident angle outside the grating $\theta_i$ and on the illumination wavelength $\lambda$. Notice that a monochromatic plane wave under Bragg angle reduces to zero the function $\vartheta(\theta_i,\lambda)$. Off-Bragg incidences give rise to $\vartheta(\theta_i,\lambda)\neq 0$ and the diffracted complex field is generated with a detuning proportional to $\vartheta(\theta_i,\lambda)$ and the grating depth. The expression of the diffraction efficiency, $\eta(\theta_i,\lambda)$, is [24]:

$$\eta(\theta_i,\lambda)=\frac{\sin^2\left[\sqrt{\nu(\theta_i,\lambda)^2+\xi(\theta_i,\lambda)^2}\right]}{1+\frac{\xi(\theta_i,\lambda)^2}{\nu(\theta_i,\lambda)^2}}, \tag{3}$$

where the functions $\nu(\theta_i,\lambda)$ and $\xi(\theta_i,\lambda)$ are defined as

$$\nu(\theta_i,\lambda)=\frac{\pi\Delta nT}{\lambda\cos\theta(\theta_i,\lambda)}, \tag{4}$$

$$\xi(\theta_i,\lambda)=\frac{\vartheta(\theta_i,\lambda)T}{2\cos\theta(\theta_i,\lambda)}, \tag{5}$$

$\eta(\theta_i,\lambda)$ represents the ratio between the diffracted intensity and the incident intensity, per unit wavelength. Diffraction efficiency as a function of $\lambda$ for a constant $\theta_i$ has a shape proportional to a quadratic sinc function, where the maximum is reach under Bragg incidence. The full-width half-maximum (FWHM) of this function is defined as the grating bandwidth, $\Delta\lambda_G$, that match the spectral width between the Bragg condition and the first minimum ($\lambda_m$) in (3). To calculate $\Delta\lambda_G$ let us make the following assumption: 1) The incoming pulse is under Bragg incidence for its central wavelength $\lambda_c$, therefore $2\Lambda\sin\theta_i=\lambda_c$ and $\xi(\theta_i,\lambda_c)=0$. In this case Eq. (2) can be written as $\vartheta(\theta_i,\lambda)=\pi\frac{\lambda_c-\lambda}{n_0(\lambda)\Lambda^2}$; 2). The diffraction efficiency under Bragg incidence reaches the maximum value ($\eta(\theta_i,\lambda_c)=1$), thus $\nu(\theta_i,\lambda_c)=\frac{\pi}{2}$. According to Eq. (3), the first minimum in the spectral selectivity curve occurs when $\xi(\theta_i,\lambda_m)=\frac{\pi\sqrt{3}}{2}$ and the grating bandwidth is:

$$\Delta\lambda_G=\lambda_c-\lambda_m=\frac{\sqrt{3}}{2}\frac{\Lambda}{T}\sqrt{(2n(\lambda_c)\Lambda)^2-\lambda_c^2}. \tag{6}$$

In Eq. (6) we have considered $n(\lambda_m)\sim n(\lambda_c)$. In the cases in which $\frac{\lambda_c}{\Lambda}\ll 2n(\lambda_c)$, Eq. (6) can be written as:

$$\Delta\lambda_G\sim 2\sqrt{3\pi}\frac{\lambda_c}{Q}, \tag{7}$$

and the grating bandwidth is inversely proportional to the parameter $Q$. A carefully selection of $Q$ will define the grating bandwidth.

The main features of the diffracted beams are determinate by the grating properties as well as the incoming pulse characteristics. We can define the diffracted spectral intensity per unit wavelength, $I_D(\theta_i,\lambda)$ through the expression:

#136396 - $15.00 USD Received 11 Oct 2010; revised 3 Dec 2010; accepted 6 Dec 2010; published 13 Jan 2011
(C) 2011 OSA

$$I_D(\theta_i,\lambda) = g(\lambda)\eta(\theta_i,\lambda), \tag{8}$$

where $g(\lambda)$ is the Gaussian shaped spectral intensity of the incident pulse, having a bandwidth $\Delta\lambda_P$ given by the FWHM of $g(\lambda)$. According to Eq. (8), gratings that satisfy $\Delta\lambda_G >> \Delta\lambda_P$ preserve the pulse spectrum, meanwhile $\Delta\lambda_G < \Delta\lambda_P$ perform a wavelengths selectivity. This criterion will be used in the next section for spectral pulse shaping.

The total diffraction efficiency of the ultrashort pulse, $\eta_T(\theta_i)$, takes into account the contribution of the whole spectrum through this expression:

$$\eta_T(\theta_i) = \frac{\int_0^\infty g(\lambda)\eta(\theta_i,\lambda)d\lambda}{\int_0^\infty g(\lambda)d\lambda}. \tag{9}$$

The representation of $\eta_T(\theta_i)$ as a function of the incidence angle $\theta_i$ outside the grating is denominated the angular selectivity curve (ASC). When $\Delta\lambda_G >> \Delta\lambda_P$, $\eta(\theta_i,\lambda)$ can be regarded as constant in the spectral interval in which $g(\lambda)$ is defined and Eq. (9) can be written as $\eta_T(\theta_i) \sim \eta(\theta_i,\lambda_c)$. The ASC is identical to that for monochromatic light. Hence the pulse characteristics are not detectable and the ASC shape is defined only by the grating properties. The opposite case occurs when $\Delta\lambda_G << \Delta\lambda_P$. In this case, $\eta(\theta_i,\lambda) \neq 0$ only for the wavelength $\lambda_i$ that satisfies the Bragg angle $\theta_i$: $2\Lambda\sin\theta_i = \lambda_i$. $\eta(\theta_i,\lambda)$ can be regarded as a delta-like function centered in $\lambda_i$ and the total diffraction efficiency is:

$$\eta\left[\theta_i(\lambda_i)\right] = \frac{b\,g(\lambda_i)}{\int_0^\infty g(\lambda)d\lambda}. \tag{10}$$

$b$ is a constant normalizing factor and the integral in the denominator takes also a constant value. Using the Bragg's law to express the incidence angle $\theta_i$ in its corresponding Bragg wavelength $\lambda_i$, the ASC reproduces the shape of the power spectrum associated to the incident pulse. Therefore, the grating characteristics are not detectable. In typical situations, the grating properties are not in the extreme cases analyzed, and the shape of the ASC is formed by a combination of both, the grating properties and the pulse power spectrum. In the following section we will use Eqs. (8) and (9) to fit and interpret the experimental results.

## 4. Experimental results

The VPHGs recorded in the photopolymerizable glass were tested with ultrashort pulses from an Amplified Ti: sapphire laser system (ATLS) delivering 50fs, 3.6mJ pulses centered at 800nm with 1KHz repetition rate. The second harmonic generation of the laser is achieved by using a non-linear crystal BBO to obtain pulses centered at 400 nm, which also have been used to analyze the diffraction features originated by the gratings.

Two types of experiments were carried out to demonstrate the pulse spectrum preservation or filtering. In the first one, the diffracted and the incident intensity per unit wavelength was measured using a portable spectrophotometer. In the second experiment, the total diffraction efficiency was obtained by normalizing the diffracted power spectrum by the addition of the transmitted and diffracted power spectra. This normalization is commonly used in holography and it does not take into account losses by Fresnel reflection. The measurements were carried out with a two-channel photodetector to collect the total transmitted and diffracted power spectra. The sample was placed on a high precision rotation stage (0.001 degrees) controlled by a computer that allow as to change the incident angle of the incoming pulses and to

#136396 - $15.00 USD Received 11 Oct 2010; revised 3 Dec 2010; accepted 6 Dec 2010; published 13 Jan 2011
(C) 2011 OSA

perform the angular selective curves. In the following, pulses centered at 800 and 400 nm will be denominated pulses *a* and *b*, respectively.

*4.1 Gratings for pulse spectral conservation*

In this section we design holographic gratings for pulse spectral conservation of the fundamental emission of the ATLS and its second harmonic, operating with maximum diffraction efficiency. To make an appropriated grating design it is necessary to know the spectral intensity per unit wavelength of the incoming pulses, $g(\lambda)$, and their spectral bandwidths $\Delta\lambda_P$. The black lines in Figs. 1(a) and 1(b) provide the normalized experimental results $g_{a,b}(\lambda)$ for pulses *a* and *b*, delivering $\Delta\lambda_{P,a} = 25nm$ and $\Delta\lambda_{P,b} \sim 7nm$. The Gratings 1 and 2, shown in Table 1, have been used to perform the experiments with pulses *a* and *b*, respectively. To know the gratings bandwidth operability we use Eq. (7) and the parameters *Q* displayed in Table 1, obtaining $\Delta\lambda_{G,1} = 130nm \gg \Delta\lambda_{P,a}$ and $\Delta\lambda_{G,2} = 80nm \gg \Delta\lambda_{P,b}$. According to the theory, these values assure pulse spectral conservation.

**Table 1. Gratings parameters**

| | $\Lambda$ ($\mu m$) | $T$ ($\mu m$) | $\Delta n$ | $Q$ |
|---|---|---|---|---|
| Grating 1 | 2 | 80 | $4.1\text{x}10^{-3}$ | 67 |
| Grating 2 | 2 | 130 | $3.1\text{x}10^{-3}$ | 54 |
| Grating 3 | 0.5 | 90 | $3.5\text{x}10^{-3}$ | 1196 |
| Grating 4 | 0.25 | 70 | $2.6\text{x}10^{-3}$ | 1880 |

The diffracted spectral intensities per unit wavelength are shown in Fig. 1(a) and 1(b), dotted curves, and the red lines represent the theoretical fit using Eq. (8) and the grating parameters. We confirmed the spectral conservation together with the high diffraction efficiencies close to ~92% and ~95% for pulses centered at 800nm and 400nm, respectively. In the experiments, the incidence angle has been selected to satisfy the Bragg condition for the central wavelengths of pulses *a* and *b*. The total diffraction efficiency as a function of the incidence angle $\theta_i$ has been used to double check the theoretical model. In Figs. 2(a) and 2(b) are displayed the ASC for Grating 1 and 2.

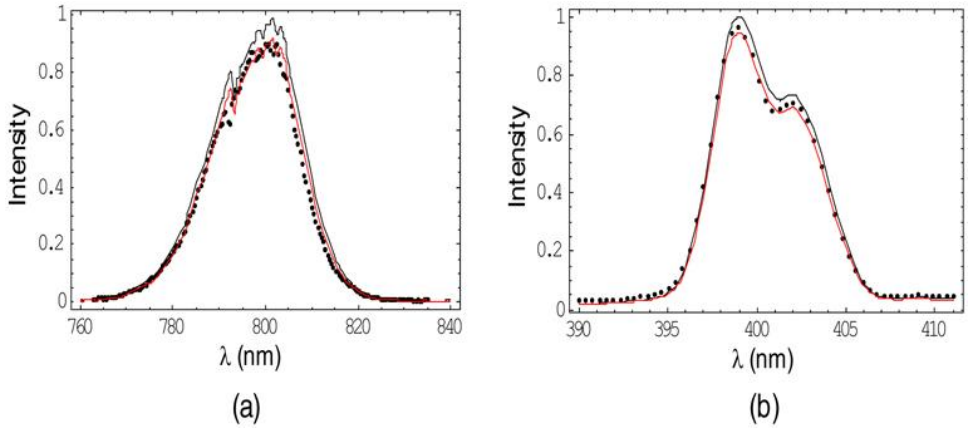


Fig. 1. Spectrum conservation of the incoming pulse: (a) Normalized spectral intensity of the fundamental emission (black line) and the diffracted pulse (dotted curve) of the ATLS system impinging Grating 1; (b) Normalized spectral intensity of the SH emission of the ATLS system (black line) and the diffracted intensity originated by Grating 2 (dotted curve). Fitting for both spectra (red lines) has been performed using Eq. (8). Grating parameters are displayed on Table 1.

#136396 - $15.00 USD Received 11 Oct 2010; revised 3 Dec 2010; accepted 6 Dec 2010; published 13 Jan 2011
(C) 2011 OSA

The shape of the ASCs resemble to the one associated to a quasi-monochromatic light, for which it is possible to resolve secondary maxima and minima. The pulse characteristics are not detectable and the ASC shape is defined only by the grating properties. This result is in accordance with the behavior predicted by the model when the condition $\Delta\lambda_G \gg \Delta\lambda_P$ is satisfied. The red lines in the figures represent the fitting using Eq. (9) and parameters in Table 1, demonstrating an excellent correspondence.

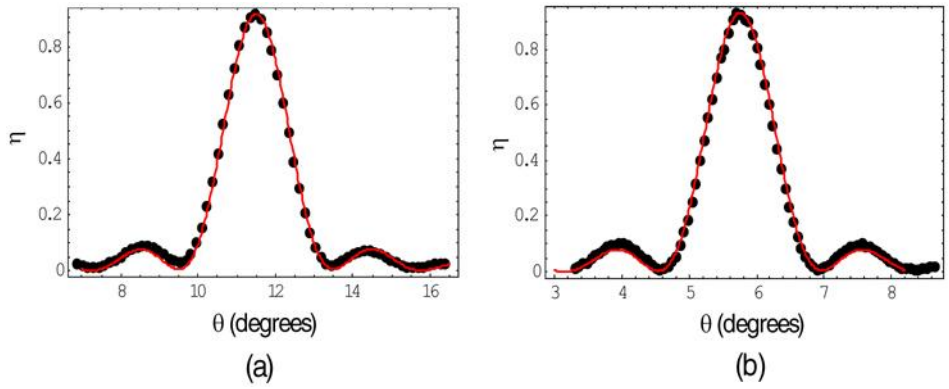


Fig. 2. Angular selectivity curves corresponding to Grating 1 (a) and 2 (b) for illumination with the fundamental emission of the ATLS system and its second harmonic, respectively. Red lines are the fitting using Eq. (9) and parameters on Table 1.

The gratings analyzed are ideal candidates for ultrashort pulses manipulation when the complete spectrum must be preserved. They involve diffractive optical elements for temporal and spatial pulse shaping. A typical arrangement for temporal pulse shaping is composed by four or pair identical gratings, as it is discussed in [6] that would be suitable to bring up the out-going pulses to its transform-limited duration. The estimated efficiency of the optical system performed with these gratings (without considering losses by Fresnel reflections) is ~72% and ~82% for the fundamental and SH pulses of the ATLS, respectively. These estimated values show an excellent potential of the optical set-up by using VPHGs in the photopolymerizable glass.

*4.2 Gratings for pulse spectral filtering*

VPHGs with narrow bandwidth operability were also recorded in the photopolymerizable glass. In order to provide an illustrative example, we have designed two spectral filters, one for the fundamental and another one for the first harmonic of the ATLS, capable to reduce four times the bandwidth of the incident spectrum. This condition is achieved if $\Delta\lambda_G \sim \frac{1}{4}\Delta\lambda_P$. These spectral filters are variable ones in the sense that the central wavelength $\lambda_i$ of the diffracted beam is selected changing the angle of incidence $\theta_i$. Specifically, $\lambda_i$ must satisfies the Bragg condition. Notice that, for pulses centered at 800 nm, $\Delta\lambda_{P,a} = 25nm$, while for pulses centered in 400 nm, $\Delta\lambda_{P,b} \sim 7nm$. The Gratings 3 and 4 shown in Table 1 have been used to perform the experiments with pulses *a* and *b*, respectively. According to Eq. (7), $\Delta\lambda_{G,3} \sim 7nm$ and $\Delta\lambda_{G,4} \sim 2nm$.

As illustrative example, in Fig. 3(a) and 3(b) we display the normalized spectral intensity of the incidence pulses *a* and *b* (black lines) and the diffracted beams (dotted lines) at different angles of incidence $\theta_i$. The angle values select the central wavelength $\lambda_i$ of the diffracted beams according to Bragg's law. The ($\theta_i$, $\lambda_i$) correspondence is shown in the figure caption, while the gratings parameters are displayed on Table 1. We stress the high diffraction efficiency delivered for a single wavelength since the spectral intensity associated with $\lambda_i$

#136396 - $15.00 USD Received 11 Oct 2010; revised 3 Dec 2010; accepted 6 Dec 2010; published 13 Jan 2011
(C) 2011 OSA

approximates the spectrum envelope at this point. The diffracted beams FWHM for pulses centered at 800 nm and 400 nm are ~6 nm and ~2 nm, respectively. These values correspond to ~25% of the $\Delta\lambda_{P,a}$ and $\Delta\lambda_{P,b}$, in accordance to the gratings design. The color lines in Figs. 3(a) and 3(b) are the theoretical results using Eq. (8) and parameters in Table 1. Notice that secondary maxima and minima are predicted by the theory, but they are partially resolved in the experiments. The slightly smoothness occurs due to small thickness gradient (~2%) in the sample. Nevertheless, there is a well correspondence between theory and experiments.

In Fig. 4(a) and 4(b) it is shown the angular selectivity curves associated to pulses *a* and *b*, respectively, and the fitting to the experimental results. The shapes of the curves are alike to the spectral intensity profiles of the corresponding incoming pulses. This fact has been predicted by the theory and it becomes more appreciable for gratings that satisfy $\Delta\lambda_G << \Delta\lambda_P$. Notice that the slightly asymmetry of Fig. 4(b) is in accordance to the spectrum shape of pulse *b*. The maximum value of the total diffraction efficiency for gratings that perform spectral filtering is always smaller than one, even if the gratings are high efficient for a single wavelength (see Eq. (9)), as the cases shown in Fig. 3. Finally, the small thickness gradient does not change appreciably the ASC´s shape since each single point on the curve is the contribution of the whole diffracted spectra at one angle of incidence.

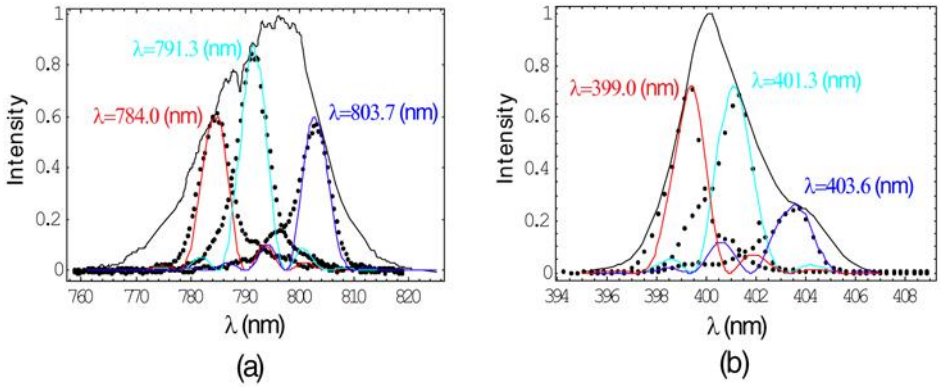


Fig. 3. (a) Normalized spectral intensity of the fundamental emission (black line) and the diffracted pulses (dotted lines) of the ATLS system impinging Grating 3 at different incident angles, ($\theta_i$ = 51.62°, $\lambda_i$ = 784.0 nm), ($\theta_i$ = 52.31°, $\lambda_i$ = 791.3 nm) and ($\theta_i$ = 53.48°, $\lambda_i$ = 803.7 nm); (b) Normalized spectral intensity of the SH emission of the ATLS system (black line) and the diffracted beams (dotted lines) by Grating 4 at different incident angles ($\theta_i$ = 32.14°, $\lambda_i$ = 399.0 nm), ($\theta_i$ = 32.35°, $\lambda_i$ = 401.3 nm), ($\theta_i$ = 32.56°, $\lambda_i$ = 403.6 nm). The color lines are the theoretical fits using Eq. (8) and the grating parameters are displayed on Table 1.

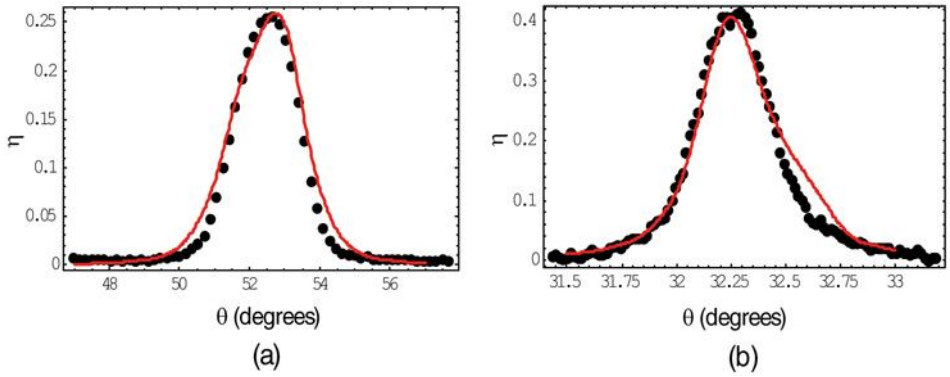


Fig. 4. Angular selectivity curves corresponding to Grating 3 (a) and 4 (b) for illumination with the fundamental emission of the ATLS system and its second harmonic, respectively. Red lines are the fitting using Eq. (9) and parameters on Table 1.

#136396 - $15.00 USD Received 11 Oct 2010; revised 3 Dec 2010; accepted 6 Dec 2010; published 13 Jan 2011
(C) 2011 OSA

According to Figs. 1–4, we conclude that the theoretical model predicts satisfactory the experimental results for both cases, gratings with wide and narrow spectral bandwidth operation, when the spectral distribution of the diffracted beam and the total diffracted power are analyzed. This indicates that undesired effects non-covered by the Kogelnik's theory like nonlinear effects are negligible in the gratings recorded in the photopolymerizable glass, up to the fluencies proven in these experiments.

We would like to mention that Grating 4 has been recorded using an alternative arrangement arrangement. The narrow grating period, $\Lambda = 0.25$ μm, induces high values of $Q$ capable to filter out the incoming pulse spectrum of the SH of the ATLS. The incidence angle of the writing beams to record such a grating can only be achieved if the photopolymerizable glass material is sandwiched between two right-angle prisms, as explained in [23]. Bragg angle for the incoming pulses with central wavelength $\lambda_c = 400$nm corresponds to a 19° incidence angle on the interface air-prism. The dispersion originated in the interface air-prism has been considered in the theoretical model. Hence, the angles $\theta_i$ displayed on Fig. 3 and 4, are measured inside the recording photomaterial.

## 5. Femtosecond laser induced damage threshold in photopolymerizable glasses

One of the core issues in development VPHGs is their laser-induced damage threshold [14–16]. In this section we analyze the LIDT for the photopolymerizable glasses in order to define the applicability range when it is used to manipulate high power ultrashort laser pulses. For this purpose, we have used VPHGs with thickness of 145 μm and a single period of $\Lambda$ = 2 μm. The LIDT experiments have been performed with an Amplified Ti: sapphire laser system delivering 50fs pulses centered at 800nm with 1 KHz repetition rate.

The incident pulses on the sample have spatial Gaussian-distribution of 2.0 mm FWHM, reached after passing by plano-convex lens with a 100cm focal-length. A variable neutral density filter was installed in the beam's path to provide energy control. The LIDT was tested with the temporal evolution of the first order diffraction efficiency of a nonactinic He–Ne laser ($\lambda$ = 632nm) probe beam during sample irradiation. The angle of incidence of the probe beam as well as the ultrashort pulses were chosen to fulfill Bragg`s condition on the same volume of the grating, see Fig. 5. In all experiments, an appropriate air absorption mechanism was activated in order to avoid breading molecules generated by evaporation and by a possible laser ablation.

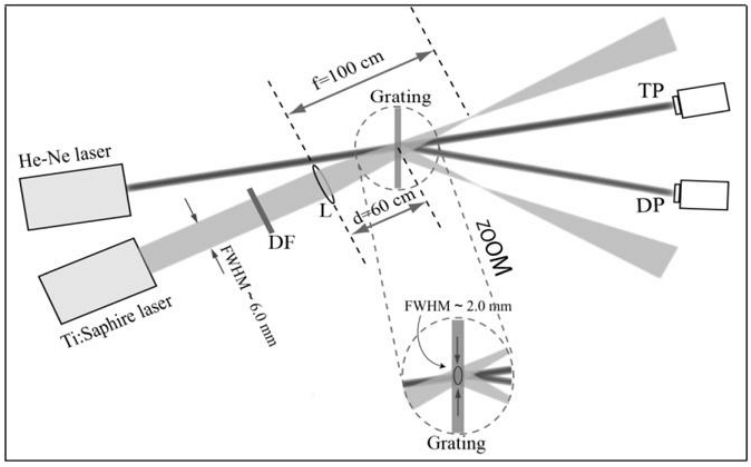


Fig. 5. Optical setup for laser induced damage threshold procedure. **DF** is a variable neutral density filter to provide energy control, (**L**) is a fused silica plano-convex lens with f = 100 cm and Φ = 1 inch, **d** is the distance between the lens and the grating (60 cm). The measurements were carried out with a two-channel photodetector to collect the total transmitted (**TP**) and diffracted (**DP**) power.

#136396 - $15.00 USD Received 11 Oct 2010; revised 3 Dec 2010; accepted 6 Dec 2010; published 13 Jan 2011
(C) 2011 OSA

The conditions were unaltered during the experiments and different tests have been performed varying the incident energy over the gratings from 0.6mJ to 1mJ per pulse. In Fig. 6 we report the evolution of the first order diffraction efficiency of the probe beam for different pulse energies. The diffraction efficiency of the gratings was obtained dividing the diffracted power by the addition of the transmitted and diffracted power. The measurements were carried out with a two-channel photodetector to collect the transmitted and diffracted power.

In all cases analyzed, but the corresponding to 0.6 mJ, the diffraction efficiency keeps constant until a critical time in which the efficiency decline and the sample exhibits damage. Data corresponding to the first 10 seconds for each curve in Fig. 6 were taking before irradiation, showing that the diffraction efficiency is constant until damage occurs. Similarly, the last 10 seconds for each experiment shows the efficiency after irradiation. It also takes a constant value equal to the one reached at the last pulse. Notice that incident pulses of 1 mJ energy (~1.25 TW/cm$^2$ per pulse) at 1 KHz repetition rate induce damage after more than $10^6$ pulses. On the contrary, sample properties remain unaltered after $10^7$ pulses of 0.6 mJ (~0.75 TW/cm$^2$ per pulse). This energy represents the upper limit of the LIDT for the volume phase holographic gratings recorded in the photopolymerizable glasses.

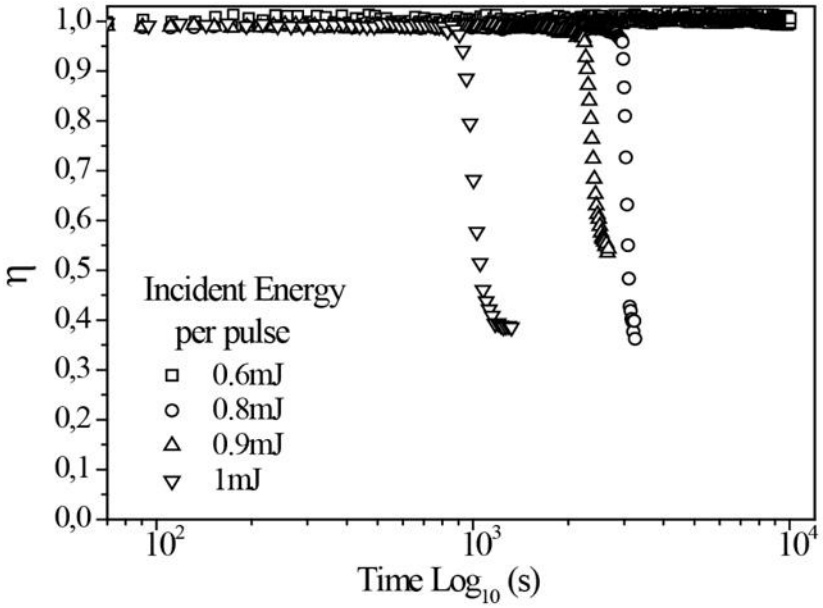


Fig. 6. Dependence of the Diffraction Efficiency on time exposition changing the incidence energy for each VPHG.

When damage occurs, the irradiated area of the sample is gradually changed from transparent to a highly absorbing circular spot whose diameter increases with exposition. At the final stage the diameter is 2 mm. Figure 7(a) is a photograph of the damaged area and Fig. 7(b) is a magnified photograph using an optical microscope (10x), showing the damage in more detail. The spot shape and dimension coincide with the spatial distribution of ~2 mm FWHM pulses, in accordance with intensity shape measurements on the sample. The dark spot absorb light generating a heat expansion that induces cracking in much more extended areas; see Figs. 7(a) and 7(b). This behavior has also been reported for femtosecond laser induce damage in highly transparent materials [27,28]. Accordingly, the photopolymerizable glass shows an excellent femtosecond LIDT and it is particularly promising for ultraintense and ultrashort pulse applications.

#136396 - $15.00 USD Received 11 Oct 2010; revised 3 Dec 2010; accepted 6 Dec 2010; published 13 Jan 2011
(C) 2011 OSA

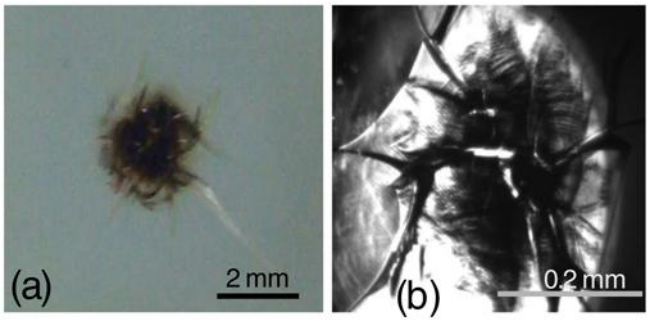


Fig. 7. (a) Photograph of the laser induced damage in the photopolymerizable glass. (b) A section of enlarged image of the damaged area with an optical microscope (10x) enhancing the details of the formation of a dark spot and the heat expansion.

## 6. Conclusion

In this paper, we explore the capability of the photopolymerizable glass to be applied in spectral manipulation of femtosecond laser pulses. For this purpose, we used VPHGs with both, wide and narrow bandwidth operations. Diffraction efficiency as well as spectral composition of the diffracted beams were analyzed for femtosecond laser pulses illumination centered at 800 nm and 400 nm, respectively. Gratings with high diffraction efficiency and high performance were implemented, showing the versatility of the photopolymerizable glass that can be exploited to design diffractive elements for temporal and spatial pulse shaping, as well as for the generation of variable spectral filters with tailored desired bandwidth operation.

We have performed experiments to determine the femtosecond laser induce damage threshold of the VPHGs implemented in the photopolymerizable glass. We have shown that the holographic material remain unaltered after more than 10 million Gaussian-shaped 50 fs pulses at 1 KHz repetition rate with a spatial FWHM of 2mm centered at 800nm and with 0.6mJ per pulse. LIDT occurs for values up to 0.75 $TW/cm^2$ indicating an excellent damage threshold. This holographic material is promising for intense-fields excitations. Meanwhile, we developed a theoretical model that takes into account the grating bandwidth operability together with the spectral bandwidth of the incoming ultrashort pulses. This model interprets the main features of the diffracted beams by VPHGs with wide and narrow spectral bandwidths. It was shown that the model fits satisfactorily the spectral composition of the diffracted pulses and the total diffraction efficiency as a function of the incidence angle, as well. We also found a suitable relation between the Klein-Cook parameter *Q* and the grating bandwidth operation (Eq. (7)) which has been used to design gratings to perform the spectral pulse shaping. As the main Kogelnik's hypotheses hold in the whole excitation range, undesired effects limiting the holographic performance seems to be negligible in this material up to fluencies close to the damage threshold.

## Acknowledgements

We thank J. A. Rodrigo and R. Weigand for helpful discussions. The financial support of the Spanish Ministry of Innovation and Science, under grant TEC2008-1045 is acknowledged. One of us (M.P. Hernandez-Garay) acknowledges the MAEC-AECID (Spain) and CONACyT (Mexico) grants, P. Vaveliuk is grateful to CNPq (Brazilian federal grant agency) for financial support. We thank to Chemical Reaction Dynamics and Femtochemistry Group: J. G. Izquierdo and L. Bañares (Spanish Ministry of Science and Innovation (MICINN) through Grant CTQ2008-02578/BQU, and Consolider SAUUL CSD2007-00013). Finally, the authors gratefully the reviewers's suggestions.

#136396 - $15.00 USD Received 11 Oct 2010; revised 3 Dec 2010; accepted 6 Dec 2010; published 13 Jan 2011
(C) 2011 OSA